Int. J. Multiphase Flow Vol. 12, No. 1, pp. 99–114, 1986
Printed in Great Britain.

0301-9322/86 $3.00 + .00

STRUCTURE OF TURBULENT BUBBLY JETS—I. METHODS AND CENTERLINE PROPERTIES

T-Y. SUN and G. M. FAETH
Department of Mechanical Engineering and The Applied Research Laboratory, The Pennsylvania State University, University Park, PA 16802, U.S.A.

(*Received* 5 *September* 1984; *in revised form* 28 *April* 1985)

Abstract—The structure of dilute bubbly turbulent round jets, injected vertically upward in still water, was studied both theoretically and experimentally. All measurements were nonintrusive, including mean and fluctuating phase velocities, bubble number intensities, bubble-size distributions and calibration of the motion of individual bubbles. Predictions from three analyses were compared with measurements: (1) locally homogeneous flow analysis, where velocity differences between the phases were neglected; (2) deterministic separated flow analysis, where relative velocity was considered but bubble/turbulence interactions were ignored; and (3) stochasic separated flow analysis, where both relative velocity and bubble/turbulence interactions were considered using random-walk methods. This paper describes theoretical and experimental methods, flow structure near the source and mean properties along the jet axis. Effects of relative velocity were important almost everywhere in the flow; therefore, only the separated flow models yielded satisfactory predictions of bubble velocities along the axis. A companion paper treats mean and fluctuating properties in other regions of the flow.

1. INTRODUCTION

Bubbly turbulent jets and plumes have a variety of applications, e.g., direct-contact heat exchangers, pressure-suppression devices, gas mixing and dissolution systems, waste treatment, bubble breakwaters, ice prevention systems in harbors, oil-well blowout, reservoir destratification and confinement of spills—among others. The present study considers a flow in this class, consisting of a dilute, turbulent, bubbly round jet injected vertically upward in a still liquid. The study provides new measurements of flow structure and analysis to assist interpretation of the measurements.

Bubbly unconfined jets and plumes have received considerable attention. Early work is reviewed by Abdel-Aal *et al.* (1966) who also report void volumes, measured nonintrusively, in the dilute region of bubbly plumes. Other workers used probes to measure mean properties, e.g., Goldschmidt *et al.* (1971), Goossens & Smith (1978) and Milgram (1983). Goldschmidt *et al.* (1971) measure turbulence properties in very dilute bubbly jets (maximum void fraction of 0.4%), and suggest that even at these conditions, continuous-phase turbulence properties are modified by bubbles. Chesters *et al.* (1980) use laser Doppler anemometry (LDA) and a double-electrode probe to measure mean liquid and bubble velocities in bubbly plumes.

Durst and coworkers have shown that LDA can measure velocities of both phases even though bubbles are larger than the LDA measuring volume: cf. Martin *et al.* (1981), and references cited therein. Several studies of individual bubble processes have followed using LDA, e.g., Mahalingam *et al.* (1976) and Brankovic *et al.* (1984); however, comprehensive measurements of phase velocities in bubbly jets and plumes have not been reported to our knowledge.

Past analysis of bubbly jets and plumes was based on classical integral models of single-phase flows, e.g., Turner (1969). Chesters *et al.* (1980) and McDougall (1978), as well as references cited therein, represent recent efforts along these lines. This is efficient for gaining a general understanding of bubbly jets and plumes; however, integral analysis provides little information on flow structure, e.g., distributions of phase velocities, etc.

The present investigation uses both theoretical and experimental methods to study the structure of turbulent bubbly jets and plumes. Measurements included mean and fluctuating

phase velocities and the Reynolds stress of the liquid phase, using LDA; the distribution of bubbles and bubble sizes, using flash photography; and calibration of individual bubble motion, using both methods. Steady axisymmetric turbulent flows, produced by injecting a bubbly air/water mixture vertically upward in still water, were studied. The flows were dilute, with maximum void fractions less than 10%, and had nearly monodisperse bubbles, roughly 1 mm in diameter. Baseline tests for pure liquid jets, using the same injector, were also completed. Special effort was made to measure near-source conditions in the flow, so that the results would be useful for evaluation of analysis.

Analysis involved evaluation of methods recently considered in this laboratory for particle-laden gas jets (Shuen *et al.* 1983, 1983a, 1985). This was of interest, since bubbly flows introduce effects of interphase momentum exchange due to virtual mass and Basset forces which are negligible in particle-laden gas jets. Three methods were considered: (1) locally homogeneous flow (LHF) analysis, where velocity differences between the phases were ignored; (2) deterministic separated flow (DSF) analysis, where relative velocity was considered in the mean, but effects of turbulence/bubble interactions were ignored; and (3) stochastic separated flow (SSF) analysis, where both relative velocity and bubble/turbulence interactions were considered using random-walk calculations of bubble motion. Similar to Shuen *et al.* (1983, 1983a, 1985), a k-ϵ model was used to represent the turbulence properties of the continuous phase. The limitations of models of this type have been extensively documented; however, they provide a reasonable representation of the structure of single-phase jets and a convenient formalism for dealing with multiphase processes, where some sort of modeling, or averaging over dispersed-phase/continuous-phase interactions, is required at present.

This paper describes experimental and theoretical methods; calibration results for the motion of individual bubbles and for single-phase liquid jets; and near-source properties and mean properties along the axis of the bubbly jets. A companion paper summarizes the remaining measurements as well as sensitivity analysis of effects of uncertainties of initial conditions and analysis parameters (Sun & Faeth 1985). The present discussion is brief, more details and a complete tabulation of data are provided by Sun (1985).

2. EXPERIMENTAL METHODS

2.1 *Apparatus*

Test tank. Water and low void fraction water–air mixtures were injected vertically upward in still water within a windowed tank (913 mm high, 534 mm wide with a length of 410 mm along the optical axis). The front and back surfaces of the tank were constructed of 5-mm-thick plate glass to provide optical access. The region where measurements were made was roughly at the tank centerline about 210 mm below the liquid surface. Water overflow was removed from the tank through a standpipe.

Instrumentation was rigid; therefore, the injector was supported on a three-directional traversing system. Horizontal and vertical positioning of the injector were accurate to 0.1 and 0.5 mm. Jet orientation was checked by matching jet centerline determinations (from measurements of Reynolds stress) with a plumb bob centered at the axis of the injector.

Injector. A cross-sectional view of the injector appears in figure 1. The exit diameter of the injector was 5.08 mm. Air was introduced from a plenum at the bottom of the injector through five hypodermic needles (22 gauge, 44 mm long) which were cut and ground to have square terminations. The downstream ends of the needles were in the plane of the inlet of the contraction section of the injector. The spacing of the needles is shown in section A-A of figure 1. Water entered a plenum just above the air plenum and passed through a screen (0.25-mm diameter wires, square pattern, 1700 wires/m) and a 14.1:1 flow area contraction before reaching the injector exit.

This arrangement provided nearly monodisperse bubbles (roughly 1 mm in diameter)

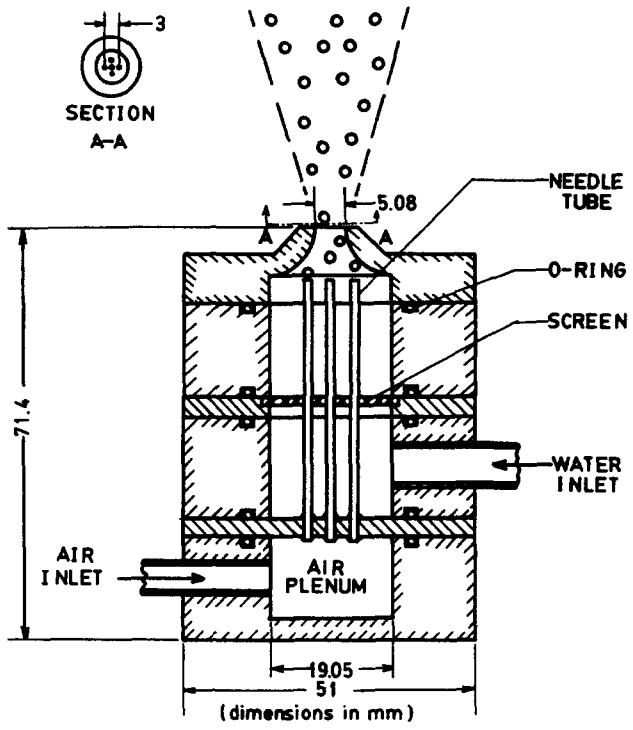

Figure 1. Sketch of the injector.

over the present test range. A critical factor for producing nearly monodisperse bubble sizes and preventing their subsequent coalescence in the flow, however, was the addition of Kodak Photo-Flo 200 solution to the water (310 μl of solution per l of water).

Flow system. Since the measurements required lengthy operation of the apparatus, the water flow from the injector was recirculated in order to conserve Photo-Flo solution. The injector flow rate was controlled by a valve and bypass system. A surge tank (1300 ml volume roughly half-filled with water) was placed in the pump outlet line to control pressure oscillations. The liquid flow rate was measured with a rotameter which was calibrated by weighing water collected for timed intervals.

Air was supplied from a commercial cylinder (99.9% purity) through a two-stage pressure regulator and a filter before entering the injector supply line. The air flow was metered using a critical-flow orifice in conjunction with a 0.2 MPa (0.01% accuracy) Bourdon gauge. The critical-flow orifice was calibrated with a bubble flow meter.

2.2 *Instrumentation*

Liquid-phase velocities. Mean and fluctuating liquid-phase velocities were measured using a single-channel LDA. Various beam orientations were used to measure components of mean and fluctuating velocities, and Reynolds stresses, following Durst & Whitelaw (1971). A 5-mW HeNe laser was used, in the dual-beam forward-scatter mode, with one beam frequency-shifted 40 MHz to eliminate errors due to flow reversals and directional bias. The optical arrangement yielded a measuring volume having a diameter and a length of 260 and 250 μm and a fringe spacing, verified by calibration with a rotating disk, of 3.29 μm.

Natural seeding contained in local tap water was sufficient to provide relatively high signal rates, e.g., 500–800 Hz. Large-amplitude signals, due to bubbles, were rejected using the amplitude-limiter on the burst-counter signal processor (sample rates for bubbles were 20–100 Hz and their bias, even if included, would be small). The signal rate was high enough to resolve the smallest scales of the flow; therefore, the analog output of the processor was

time-averaged with an integrating digital voltmeter. Fluctuating velocities were averaged in the same manner, after processing the signal with a true rms meter. Sampling times of 5–10 min were used to obtain stable averages.

Errors due to directional bias and directional ambiguity were eliminated by frequency shifting, while effects of gradient bias were small, less than 1%. Analysis indicated uncertainties in mean and fluctuating velocities less than 5% (95% confidence interval) and less than 10% for k. Uncertainties in Reynolds stress were greater, e.g., less than 18% at the position of maximum Reynolds stress, with proportionately higher uncertainties for lower values of Reynolds stress. All results were repeatable within these limits over the period of months during which the measurements were made.

Bubble-phase velocities. The LDA was modified to measure bubble-phase velocities. Beam spacing was reduced, yielding a calibrated fringe spacing of 19.6 μm, while the receiving optics were shifted to 45° from the optical axis in the forward-scatter direction. This yielded an optical measuring volume having a 260 μm diameter and a 260 μm length. Grazing collisions were recorded; therefore, a better estimate of the size of the measuring volume is the sum of the optical and bubble diameters. One beam was frequency-shifted 40 MHz to eliminate effects of velocity bias and directional ambiguity.

The detector was operated at low gain so that only large-amplitude signals from bubbles were recorded. The burst-counter signal processor was used in both time- and bubble-averaging modes. Only the latter are reported here, although both results were nearly identical. Bubble-averaged data was obtained by storing and processing the digital output of the counter with a DEC MINC 11/23 minicomputer. A sample of 500–3000 bubbles was used to yield number-averaged mean, $\overline{u}_p$, and fluctuating, $\overline{u}'_p$, velocities. Occasional erroneous signals were eliminated by rejecting all data lying outside $\pm 10\ \overline{u}'_p$ of the mean bubble velocity.

Effects of gradient biasing for mean bubble velocities were less than 1%. Gradient biasing for bubble velocity fluctuations reached at value of 8% for the highest initial void fraction flow, at $x/d = 8$, where x is height above the injector and d is the injector exit diameter. At other axial stations, gradient biasing errors were less than 1%. Uncertainties in mean and fluctuating bubble velocities were less than 5%.

Bubble size and distribution. Flash photography was used to measure bubble size and distribution in the flow. The light source for the photographs was a General Radio, model 1538-A Strobotac, operated in the manual mode and positioned near the camera. The photographs were taken with a Graflex 4 × 5 camera with a 135-mm lens located 500 mm from the jet axis. The depth of field extended beyond the depth of the flow and parallax errors are less than 7%; therefore, bubbles from the entire line-of-sight through the flow were recorded. The pictures were taken in a darkened room with an open shutter (Polaroid, type 57 film); therefore, the exposure time was fixed by the flash duration (less than 1 μs) which effectively stopped bubble motion. Bubbles were sized and counted by viewing the photographs under a microscope.

Bubble sizes did not change appreciably in the flow; therefore, they were found by measuring at least 1000 bubbles over the entire field. The Sauter (SMD), volume (VMD) and number (NMD) mean diameters and the standard deviation of the VMD were evaluated from their standard definitions (Sun 1985).

Bubble distributions were represented by bubble number intensities, e.g., the number of bubbles per unit area of a line-of-sight observation through the flow. This measurement could be deconvoluted to give bubble density, e.g., the number of bubbles per unit volume, but this was impractical because of limited spatial resolution and sample sizes. Bubble number intensities are still useful, however, since they are easily found from predictions for comparison with present measurements.

The uncertainty in the bubble size determination is due to diameter measuring accuracy and discretization errors for finite sample sizes. The latter reflect dominates yielding an uncertainty of 10% for SMD. Bubble number intensities are subject to gradient bias due to radial discretization of the measurements, but this was less than 12% for present test conditions. The uncertainty of the measurements due to parallax and effects of finite sample sizes was also less than 12%.

2.3 *Test conditions*

Test conditions are summarized in table 1. The presence of the Photo-Flo solution did not significantly change the bath liquid properties from water. The flows were turbulent, with initial Reynolds numbers in the range 8530–9380. In general, 90% of the bubbles had diameters within 10% of the SMD; therefore, the assumption of monodisperse bubble sizes is reasonable.

3. THEORETICAL METHODS

3.1 *General description*

Theoretical methods follow the approach developed by Shuen *et al.* (1983,1983a,1985) for particle-laden jets. Therefore, the present description is brief, stressing the major modifications needed to treat bubbly jets. The most significant changes involve the state relationships used in LHF analysis and the equations of dispersed-phase (bubble) motion used in separated flow analysis. In particular, bubble motion involves virtual mass and Basset forces which are generally negligible for the motion of solid and liquid particles in gases.

The analyses consider steady turbulent, bubbly, isothermal, air–water jet injected vertically upward in a stagnant water bath at atmospheric pressure. Both gas and liquid densities are essentially constant. Mach numbers were small; therefore, kinetic energy and viscous dissipation of the mean flow can be neglected with little error. The present flows spread similar to single-phase jets; therefore, the boundary-layer assumptions were adopted for the continuous phase.

A k-ϵ-g (LHF) or k-ϵ (DSF,SSF) turbulence model was used to find the properties of the continuous phase, where k is turbulence kinetic energy, ϵ is the rate of dissipation of

Table 1. Summary of test conditions†

Flow	Single-Phase Jet	Bubbly Jet I	Bubbly Jet II	Bubbly Jet III
Water flow rate (ml/s)	32.7	32.7	32.7	32.7
Air flow rate (ml/s)	0.	0.82	1.64	3.27
Jet volume fraction (%)	0.	2.4	4.8	9.1
Jet momentum (mN)	52.7	54.1	55.4	58.0
Jet velocity (m/s)‡	1.61	1.65	1.68	1.77
Jet Reynolds number§	8530	8740	8860	9380
Jet Richardson number × 10^4¶	0.	4.5	8.9	15.9
Bubble SMD (mm)	—	1.00	1.08	1.12
Bubble VMD (mm)	—	0.99	1.04	1.09
Bubble NMD (mm)	—	0.98	1.03	1.06
Std. dev. of NMD (mm)	—	0.11	0.14	0.16

†Injector exit diameter 5.08 mm, fluid temperature 298 ± 2 K, ambient pressure at injector exit 98 ± 3 kPa. Water bath contained 310 μl/l Kodak Photo-Flo 200 solution yielding a density of 1000 kg/m^3 and a viscosity of 99 × 10^{-5} Ns/m^2.

‡$u_o = \dot{M}_o/(\dot{m}_a + \dot{m}_w)_o$, where $\dot{M}_o$ is the injector thrust and $\dot{m}_a$ and $\dot{m}_w$ are the air and water flow rates through the injector.

§$\mathrm{Re} = u_o d/\nu_w$, where d is the injector diameter and ν_w is the kinematic viscosity of water.

¶$\mathrm{Ri} = (\rho_w - \rho_o)ad/\rho_w$, where ρ_w and ρ_o are water and injector exit densities while a is the acceleration of gravity.

turbulence kinetic energy and g is the variance of mixture fraction fluctuations. The formulation and empirical constants were evaluated for constant- and variable-density single-phase jets in this laboratory by Jeng & Faeth (1984) and Shuen *et al.* (1983,1983a,1985) and were not changed for the present study.

3.2 *LHF analysis*

The LHF approximation implies that both phases have the same instantaneous local velocity; therefore, the flow corresponds to variable-density single-phase fluid due to changes in bubble concentration, even though the density of each phase remains constant. The analysis is based on the conserved-scalar approach proposed by Lockwood & Naguib (1975), but used mass weighted (Favre)-averages following Bilger (1976) rather than time (Reynolds)-averages used in the original formulation. The formulation, empirical constants and definition of initial conditions followed past practice (Jeng & Faeth 1984; Shuen *et al.* 1985).

Structure predictions and measurements are presented as Favre-averaged properties, defined as follows:

$$\tilde{\phi} = \overline{\rho\phi}/\bar{\rho}, \qquad [1]$$

where ϕ is a generic property, ρ is density and an overbar denotes a conventional time-average. This is required in order to correctly represent predictions of the LHF model. This distinction is of little consequence for present flows, however, since maximum density variations are less than 10%.

Under the present assumptions the instantaneous concentration of bubbles and the density are only functions of mixture fraction, f, which is the fraction of mass at a point which originated from the injector. This implies that instantaneous scalar properties can be found using simple adiabatic mixing calculations, where f kg of injector fluid of $(1-f)$ kg of ambient fluid are adiabatically mixed and brought to thermodynamic equilibrium. This yields the following state relationships, required by the conserved-scalar formalism, for mixture density, bubble concentration, C, and void fraction, α:

$$1/\rho = f/\rho_0 + (1-f)/\rho_\infty, \qquad [2]$$

$$C/C_0 = f, \qquad [3]$$

$$\alpha = f\alpha_0/[f + (1-f)(\rho_0/\rho_\infty)]. \qquad [4]$$

The subscripts 0 and ∞ denote injector exit and ambient conditions. Since ρ, C and α are only functions of mixture fraction, appropriate averages can be found from the Favre probability density function (PDF) of mixture fraction. The Favre PDF of mixture fraction was taken to be a clipped-Gaussian function whose parameters were found from the solution of the governing equations following Lockwood & Naguib (1975) and Jeng & Faeth (1984).

For monodisperse bubble sizes, time-averaged void fraction is proportional to time-averaged bubble number density. This quantity was found by converting the Favre PDF of mixture fraction to the time-averaged PDF and integrating over the latter PDF, similar to Jeng & Faeth (1984). Path integrals of this property, through the flow, yielded bubble number intensities for comparison with the measurements.

3.3 *Bubble motion analysis*

Both separated flow models employ similar analysis for bubble motion. The main difference is that bubbles only interact with mean liquid properties for the DSF model, while bubbles interact with instantaneous liquid properties for the SSF model. Both separated flow analyses involve dividing the bubbles into n groups, defined by velocity and position at the

initial condition, and then computing their trajectories through the flow field by solving their Lagrangian equations of motion.

Initial conditions for separated flow analysis were specified at $x/d = 8$, which was the position nearest to the injector where all needed measurements could be made with acceptable spatial resolution and accuracy. Downstream of this position, void fractions were always less than 5%; therefore, bubble collisions were infrequent and effects of adjacent bubbles on bubble dynamics were small. Thus both effects were ignored (aside from the fact that bubbles influence the properties of the continuous phase through their source terms).

Bubble diameters were less than 10% of the flow width; therefore, bubbles were assumed to have uniform velocities throughout their volume. Bubble aspect ratios were in the range 1.0–1.2: therefore, bubbles were assumed to be spheres for analysis. Magnus and Saffman-lift forces were small in comparison to drag forces, due to the relatively small bubble sizes, and were ignored, cf. Faeth (1983), Finally, the inertia of the gas phase itself was neglected since the density ratio is roughly 800.

Under these assumptions, best available evidence is that the motion of the dispersed phase is governed by the Basset–Boussinesq–Oseen (BBO) equation for the motion of spheres at low Reynolds numbers, empirically extended to higher Reynolds numbers. The formulation used follows Odar & Hamilton (1964) as recently reviewed by Clift et al. (1978).

$$\frac{\Delta_A}{2}\frac{\mathrm{d}u_{ri}}{\mathrm{d}t} = a\delta_{ij} - \frac{3}{2}\frac{C_D}{d_p}|\,\mathbf{u}_r\,|\,u_{ri} - \Delta_H\left(\frac{81\nu}{\pi d_p}\right)^{1/2}\int_{t_0}^{t}(t-\xi)^{-1/2}\frac{\mathrm{d}u_{ri}}{\mathrm{d}\xi}\,\mathrm{d}\xi, \qquad [5]$$

where u_{ri} is the difference between bubble and liquid velocities ($i = 1,3$ for the three components of velocity with u_{r1} being vertical), $|\,\mathbf{u}_r\,|$ is the magnitude of the velocity vector, t is time, a is the gravitational acceleration, δ_{ij} is the Kronecker delta function, C_D is the drag coefficient, d_p is the bubble diameter and ν is the liquid kinematic viscosity. The term on the LHS of the equation is the virtual mass inertial term while the terms on the RHS of the equation represent buoyancy, drag and Basset history forces. Effects of pressure fluctuations have been ignored. The parameters Δ_A and Δ_H were defined empirically by Odar & Hamilton (1964). Their departure from unity, which is correct for the low Reynolds number regime of the BBO formulation, provides a means of treating accelerative effects at Reynolds numbers of interest in this investigation. Based on existing information, Δ_A and Δ_H can be correlated in terms of an acceleration parameter $(d_p/|\,\mathbf{u}_r\,|^2)(\mathrm{d}|\,\mathbf{u}_r\,|/\mathrm{d}t)$ for both sinusoidal and rectilinear motion, falling in the ranges 1.0–2.1 and 1.00–0.48, respectively (Clift *et al.* 1978).

The drag coefficient was correlated empirically using the standard correlation for solid spheres (Faeth 1983):

$$C_D = \frac{24}{\mathrm{Re}}\left(1 + \frac{\mathrm{Re}^{2/3}}{6}\right), \quad \mathrm{Re} < 1000, \qquad [6]$$

where Re is the bubble Reynolds number, based on the relative velocity and liquid properties. Methods used to complete bubble trajectory calculations follow Shuen *et al.* (1983, 1983a,1985) and are fully described by Sun (1985).

3.4 *DSF analysis*

The DSF analysis adopts the main features of the LHF model for the liquid phase, however, the conserved-scalar formalism is no longer needed and only k-ϵ turbulence analysis is used. Because of the low void fraction of the flow, the volume of the dispersed phase was ignored in the formulation with little error. The DSF approximation implies that

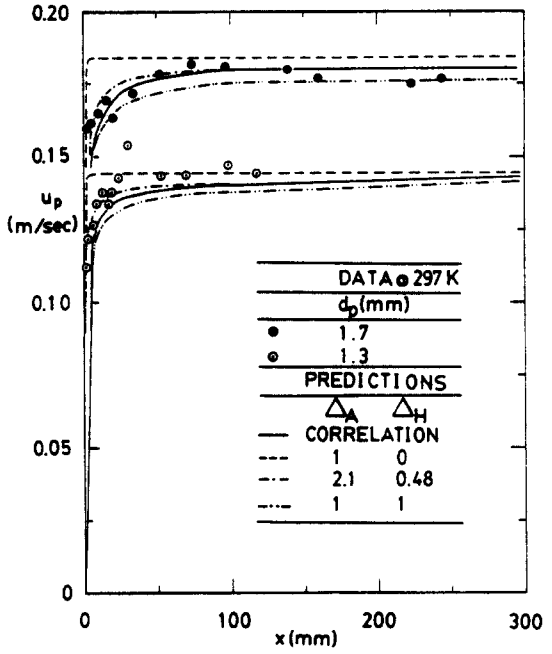

Figure 2. Single bubble trajectory calibration.

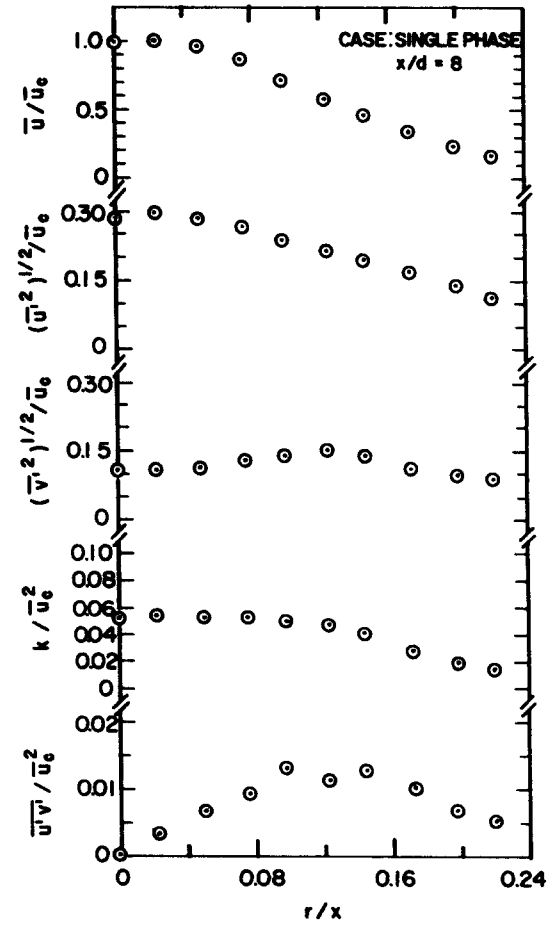

Figure 3. Mean and turbulent properties for the single-phase jet at $x/d = 8$.

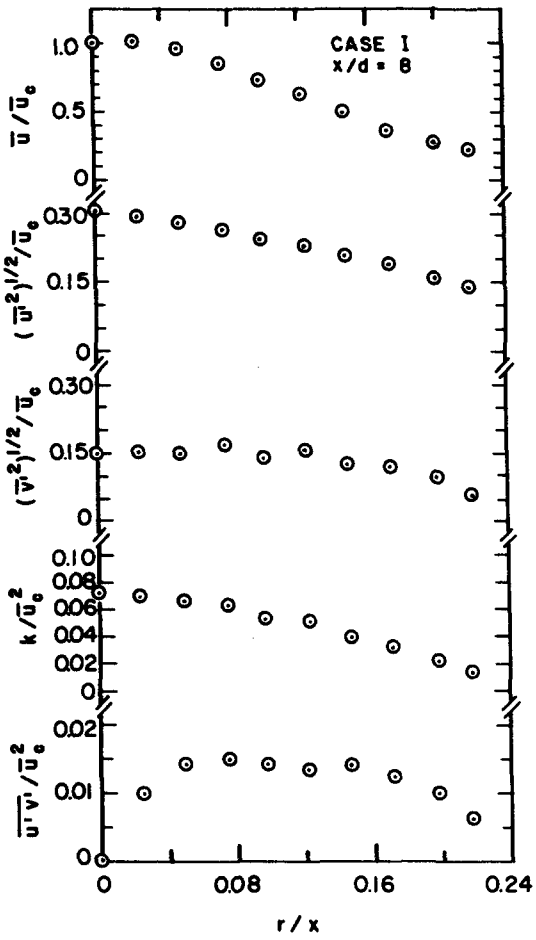

Figure 4. Mean and turbulent liquid-phase properties for the case I bubbly jet at $x/d = 8$.

bubble/turbulence interactions are ignored; therefore, bubbles only introduce a new source term in the governing equation for conservation of streamwise momentum.

The bubble source term provides the connection between the Lagrangian bubble trajectory calculations and the Eulerian continuous-phase calculations. The momentum exchange source term, S_{pu_j}, for grid node j of the continuous phase solution, is given by

$$S_{pu_j} = V_j^{-1} \sum_{i=1}^{n} \dot{n}_i m_p [u_{pi_{in}} - u_{pi_{out}} - a(\rho/\rho_p - 1)\,\Delta t_p], \qquad [7]$$

where V_j is the volume of the computational cell, $\dot{n}_i$ is the number of bubbles per unit time in group i, m_p is the bubble mass, Δt_p is the residence time of a bubble in the computational cell and "in" and "out" denote conditions entering and leaving the computational cell. The flow rate of bubbles along a given trajectory is conserved; therefore, $\dot{n}_i$ is a constant specified near the injector to satisfy total gas volume flow rate requirements. Present results were obtained by considering 400 bubble groups.

3.5 *SSF analysis*

The SSF analysis treats effects of turbulent fluctuations on interphase momentum transport using a technique proposed by Gosman & Ioannides (1981) and subsequently developed in this laboratory by Shuen *et al.* (1983,1983a,1985). This involves computing trajectories of a statistically significant number of bubbles (typically 2000) as they move away from the injector and encounter a succession of turbulent eddies.

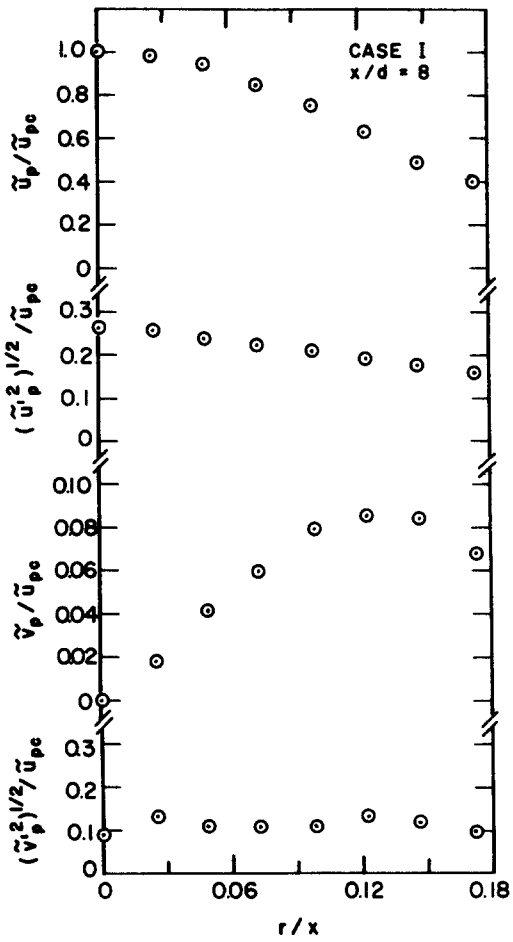

Figure 5. Mean and fluctuating bubble-phase properties for the case I bubbly jet at $x/d = 8$.

Properties within a particular eddy are assumed to be uniform, but to change from eddy to eddy. Trajectory calculations are the same as the DSF model, except that instantaneous eddy properties replace mean-liquid properties. Eddy properties are found by making a random selection from the velocity PDF–assuming isotropic turbulence. A bubble is assumed to interact with an eddy as long as its relative displacement is less than a characteristic eddy size and its time of interaction is less than a characteristic eddy lifetime. All these parameters are found directly from the k-ϵ turbulence computations, cf. Shuen *et al.* (1983,1983a,1985). Properties of the bubbles at the initial condition are also randomly sampled using measured mean and fluctuating bubble velocities and assuming Gaussian PDF's for each velocity component.

The bubble source term in the momentum equation is unchanged from the DSF analysis. Because of the low void fraction, effects of bubble source terms in the governing equations for turbulence quantities are not large and were ignored for most of the computations. However, to investigate these interactions, called turbulence modulation by Al Taweel & Landau (1977), they were also considered in a portion of the calculations following the approach of Shuen *et al.* (1985). With this approach, the bubble source term in the k-equation is exact and involves no new empiricism. The bubble source term in the ϵ-equation, however, must be modeled, yielding an empirical constant, $C_{\epsilon 3}$, whose value is not known accurately. As a result, a range of values of $C_{\epsilon 3}$ was considered to determine the sensitivity of predictions to this parameter.

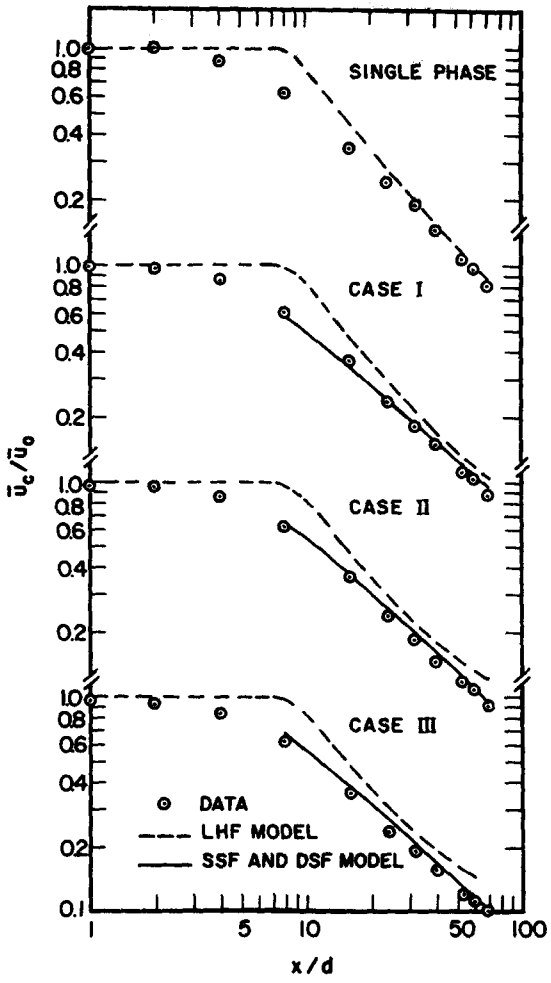

Figure 6. Mean liquid-phase velocities along the axis.

4. RESULTS AND DISCUSSION

4.1 *Trajectory calibrations*

Computation of bubble trajectories was calibrated using measurements for single bubbles rising in the bath liquid. Bubble velocities were measured, using multiflash photography, at various heights above their point of release. Bubble diameters for the calibration tests were 1.3 and 1.7 mm. Bubble generation frequencies were less than 0.2 Hz, yielding results which were independent of the generation rate.

Predicted and measured bubble velocities, as a function of distance above the point of release, are illustrated in figure 2. Predictions are shown for limiting values of Δ_A and Δ_H as well as for the correlation of Odar & Hamilton (1964). The correlation yields best results, although limiting values also yield reasonably good results. Ignoring the Basset force, by setting $\Delta_H = 0$, tends to overestimate the rate of initial acceleration of the bubble. These results indicate that present methods for computing bubble motion are adequate for subsequent calculations with bubbly jets.

4.2 *Near-injector properties*

The closest position to the injector where measurements could be made for all flows was $x/d = 8$; therefore, this position was used as the initial condition for separated flow analysis. Measurements of initial continuous-phase properties included: mean streamwise velocities, $\bar{u}$

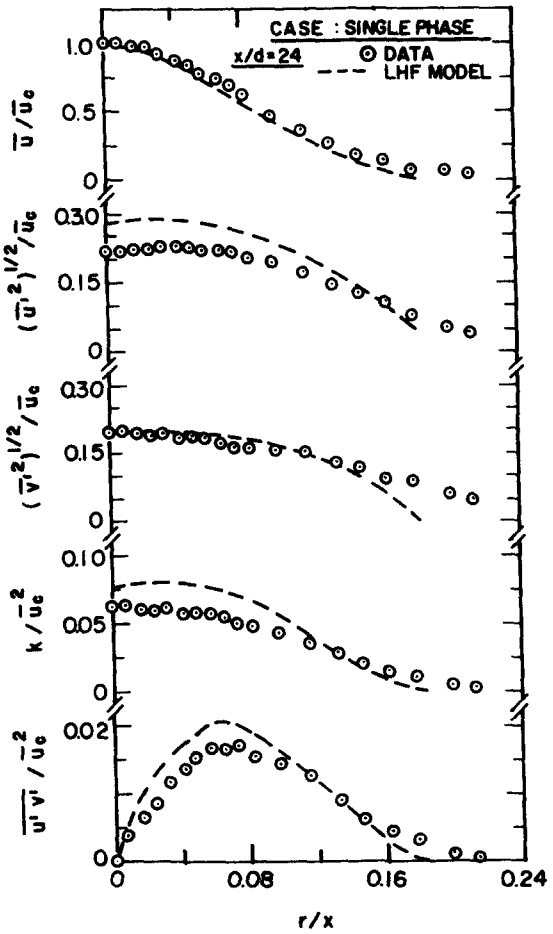

Figure 7. Mean and turbulent quantities for the single-phase jet at $x/d = 24$.

and $\bar{v}$, fluctuating streamwise and radial velocities, $\overline{u'}$, and $\overline{v'}$; and the Reynolds stress, $\overline{u'v'}$. The mean tangential velocity was zero. To complete specification of initial conditions needed by the analyses, k and ϵ must be known. k was found by assuming that radial and tangential velocity fluctuations were equal—which agreed with limited measurements. Given profiles of $\bar{u}$, $\overline{u'v'}$ and k, the initial profiles of ϵ were estimated from the definition of turbulent viscosity and the turbulence model, e.g.,

$$\epsilon = (C_\mu k^2/\overline{u'v'})\, \mathrm{d}\bar{u}/\mathrm{d}r, \qquad [8]$$

where C_μ is a turbulence model constant and r represents the radial direction.

Measurements of initial bubble-phase properties included mean and fluctuating streamwise and radial velocities, $\overline{u_p}$, $\overline{u_p'}$, $\overline{v_p}$ and $\overline{v_p'}$. Mean tangential velocities were taken to be zero while the fluctuating tangential and radial velocities were assumed to be equal. Spatial resolution was insufficient to determine void volume accurately; therefore, bubbles were assumed to be distributed uniformly over the region where they were observed. Limited evidence from the photographs suggested that this was a reasonable approximation.

Properties of the single-phase water jet at $x/d = 8$ are illustrated in figure 3. In this and following figures, radial distances are normalized by distance from the injector, which is the similarity variable for fully developed turbulent jets. Centerline quantities are designated by the subscript c. The flow is developing at this position, as indicated by relatively low values of maximum Reynolds stress and rather large flow width in terms of the radial similarity

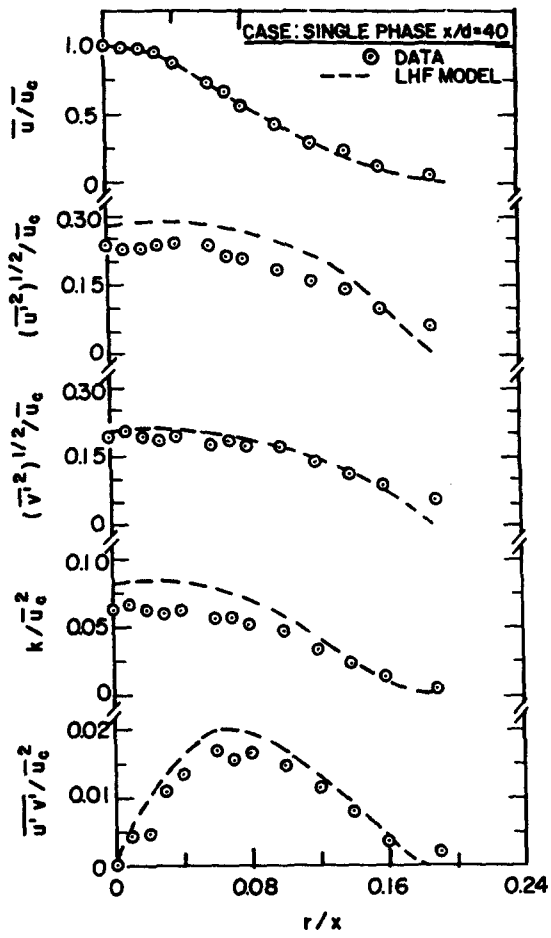

Figure 8. Mean and turbulent quantities for the single-phase jet at $x/d = 40$.

variable. Turbulence levels are high in comparison to jets from most nozzle flows, at comparable positions, due to turbulence generated by the array of capillary tubes at the inlet of the nozzle contraction.

Results for the case I flow at $x/d = 8$ are typical of the bubbly jets, cf. figure 4. In general, profiles of $\bar{u}$, $\bar{v}$ and $\overline{u}'$ were similar for the single- and two-phase jets. However, k and $\overline{v}'$ were greater in the bubble jets, perhaps due to periodic addition of bubbles at the injector exit.

Initial bubble-phase properties for case I jet are illustrated in figure 5. Mean velocity profiles, fluctuating intensity levels, and levels of anisotropy of fluctuating quantities are similar to values for the continuous phase, cf. figure 4. Mean radial bubble velocities increase from the centerline and reach a maximum near the edge of the bubble containing region. Unlike radial velocities for the continuous phase, radial bubble velocities don't become negative near the edge of the flow since no bubbles are entrained from the surroundings.

4.3 *Water jet structure*

Results of the pure liquid jet will be considered to establish some credibility for the turbulence model used to treat the continuous phase. Predicted and measured mean streamwise velocities along the axis are illustrated in figure 6. The flow exhibits a short potential core due to the relatively high turbulence levels at the injector exit. Far from the injector, however, the velocity decays inversely proportional to distance from the injector—which is expected in fully developed jets.

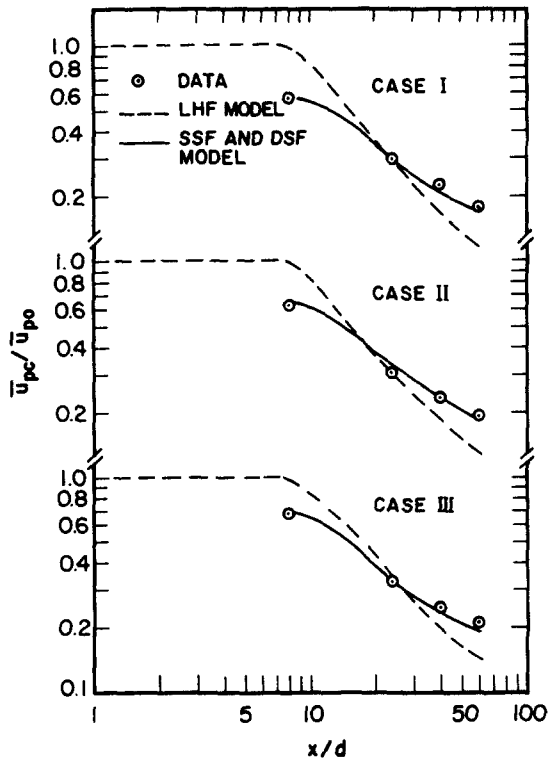

Figure 9. Mean bubble-phase velocities along the axis.

Two predictions are shown for the single-phase jet on figure 6. One uses the standard jet exit conditions for the LHF analysis while the second uses measured initial conditions at $x/d = 8$. The latter method is in good agreement with the measurements, while the former method overestimates the length of the potential core and is only in good agreement with the measurements at large x. Comparing the two predictions shows effects of uncertainties of initial conditions, clearly indicating the importance of initial condition measurements for assessment of turbulence analysis.

Figures 7 and 8 are illustrations of predicted and measured flow properties in the single-phase jet at $x/d = 24$ and 40. Predictions are for the standard LHF calculation but are virtually identical to computations begun at $x/d = 8$ with measured initial conditions. Following past practice (Shuen *et al.* 1983a,1985), the usual levels of anisotropy observed in the self-preserving region of jets were assumed, i.e. $\overline{u'^2}:\overline{v'^2} = k:k/2$ (Wygnanski & Fiedler 1969), for velocity fluctuation predictions.

Considering the somewhat ad hoc distribution of velocity fluctuations assumed for the analysis, the comparison between predictions and measurements seen in figures 6 and 7 is reasonably good. Discrepancies are generally within anticipated experimental uncertainties.

4.4 *Axial properties of bubbly jets*

Numerically closed separated flow calculations considering the Basset force term were extremely expensive and could only be undertaken in a few instances. It was found that considering this term had negligible influence on continuous-phase properties since the flows were very dilute. The Basset force term influenced bubble-phase properties by at most 5%, which is less than experimental uncertainties. Therefore, theoretical results considered subsequently all ignore Basset force effects. The low Reynolds number limit for the virtual

mass force, $\Delta_A = 1$, is used in the predictions that are pictured. Use of the other limit, $\Delta_A = 2.1$, also resulted in changes in dispersed-phase properties that were less than experimental uncertainties.

Predicted (LHF and SSF analyses) and measured values of $\bar{u}$ along the axis of the bubbly jets are illustrated in figure 6. Differences between DSF and SSF predictions were less than 1% in this case.

In figure 6, the variable-density properties of the LHF analysis cause the rate of decay of mean velocity to decrease far from the injector as a result of buoyancy forces. In general, the LHF method overestimates continuous-phase flow velocities near the injector, probably due to errors in initial conditions, similar to the effect observed for the single-phase flow. Discrepancies for LHF analysis far from the injector are due to effects of relative velocity, which become important at low liquid velocities.

In contrast, the SSF analysis agrees reasonably well with measurements illustrated in figure 6. This is due to use of actual initial conditions at $x/d = 8$ and consideration of relative velocities. Since present flows are very dilute, effects of bubbles on continuous-phase properties are not large, e.g., both measurements and predictions of continuous-phase properties for the single-phase jet and the three bubbly jets are nearly identical.

Differences between LHF and separated flow analysis are larger for bubble-phase properties. Predicted (LHF and SSF) and measured mean bubble velocities along the axis of the three bubble jets are illustrated in figure 9. Predictions of the DSF and SSF analyses were virtually identical. Bubble velocities are lower than liquid velocities near the injector, because of the bubble formation system. With increasing distance, however, bubble velocities become greater than liquid velocities due to effects of buoyancy. In the far field, bubbles are dispersed and liquid velocities are low; therefore, the bubbles approach their terminal velocities. Since the LHF analysis neglects the relative velocity, it does not reproduce any of these trends. Both separated flow models, however, yield reasonably good predictions of mean bubble velocities along the axis.

CONCLUSIONS

Final conclusions appear in the companion paper by Sun & Faeth (1985). Some initial conclusions, based on results presented thus far, are as follows:

(1) Predictions and measurements for the single-phase jet were in reasonably good agreement when measured initial conditions were used to initiate calculations.
(2) Present bubbly jets are dilute; therefore, liquid-phase properties were not strongly influenced by interphase transport and all methods of analysis yielded reasonably good predictions of these properties.
(3) Effects of relative velocity are important virtually everywhere in the present bubbly jets. Therefore, only the separated flow analyses yielded satisfactory predictions of mean bubble velocities.
(4) Trajectories of individual bubbles were best represented using correlations for Δ_A and Δ_H from Odar & Hamilton (1964).
(5) The Basset history term influences predictions less than 5% for present conditions.

Acknowledgements—This research was supported by the Office of Naval Research, Contract No. N00014-80-0517 under the technical management of R. D. Ryan. The authors also acknowledge the valuable help of L-D. Chen and J-S. Shuen during development of the analysis.

REFERENCES

ABDEL-AAL, H. K., STILES, G. B. & HOLLAND, C.D. 1966 Formation of interfacial area at high rates of gas flow through submerged orifices. *A.I.Ch.E.J.* **12,** 174–180.

AL TAWEEL, A. M. & LANDAU, J. 1977 Turbulence modulation in two-phase jets. *Int. J. Multiphase Flow* **3,** 341–351.

BILGER, R. W. 1976 Turbulent jet diffusion flames. *Prog. Energy Combust. Sci.* **1,** 87–109.

BRANKOVIC, A., CURRIE, I. G. & MARTIN, W. W. 1984 Laser-Doppler measurements of bubble plumes. *Phys. Fluids* **27,** 348–355.

CHESTERS, A. K., VAN DOORN, M. & GOOSSENS, L. H. J. 1980 A general model of unconfined bubble plumes from an extended source. *Int. J. Multiphase Flow* **6,** 499–521.

CLIFT, R., GRACE, J. R. & WEBER, M. E. 1978 *Bubbles, Drops and Particles,* pp. 185–319. Academic, New York.

DURST, F. & WHITELAW, J. H. 1971 Measurements of mean velocity, fluctuating velocity and shear stress in air using a single channel optical anemometer. *DISA Information* **12,** 11–16.

FAETH, G. M. 1983 The evaporation and combustion of sprays. *Prog. Energy Combust. Sci.* **9,** 1–76.

GOLDSCHMIDT, V. W., HOUSEHOLDER, M. K. & CHUANG, S. C. 1971 Turbulent diffusion of small particles suspended in turbulent jets. *Progress in Heat and Mass Transfer,* Vol. 6, pp. 487–508. Pergamon, Oxford.

GOSMAN, A. D. & IOANNIDES, E. 1981 Aspects of computer simulation of liquid-fueled combustors. AIAA Paper No. 81-0323.

GOOSSENS, L. H. J. & SMITH, J. M. 1975 The hydrodynamics of unconstrained bubble columns for mixing lakes and reservoirs. *Chem. Eng. Tech.* **47,** 951.

JENG, S-M. & FAETH, G. M. 1984 Species concentrations and turbulence properties in buoyant methane diffusion flames. *J. Heat Transfer* **106,** 721–727.

LOCKWOOD, F. C. & NAGUIB, A. S. 1975 The prediction of fluctuations in the properties of free, round-jet, turbulent diffusion flames. *Comb. Flame* **24,** 109–124.

MAHALINGAM, R., LIMAYE, R. S. & BRINK, J. A., JR. 1976 Velocity measurements in two-phase bubble-flow regime with laser-Doppler anemometry. *A.I.Ch.E.J.* **22,** 1152–1155.

MARTIN, W. W., ADBELMESSIH, A. H., LESKA, J. J. & DURST, F. 1981 Characteristics of laser-Doppler signals fom bubbles. *Int. J. Multiphase Flow* **7,** 439–460.

MCDOUGALL, T. J. 1978 Bubble plumes in stratified environments. *J. Fluid Mech.* **85,** 655–672.

MILGRAM, J. H. 1983 Mean flow in round bubble plumes. *J. Fluid Mech.* **133,** 345–376.

ODAR, F. & HAMILTON, W. S. 1964 Force on a sphere accelerating in a viscous fluid. *J. Fluid Mech.* **18,** 302–314.

SHUEN, J-S., CHEN, L-D. & FAETH, G. M. 1983 Evaluation of a stochastic model of particle dispersion in a turbulent round jet. *A.I.Ch.E.J.* **29,** 167–170.

SHUEN, J-S., CHEN, L-D. & FAETH, G. M. 1983a Predictions of the structure of turbulent, particle-laden, round jets. *A.I.A.A.J.* **21,** 1480–1483.

SHUEN, J-S., SOLOMON, A. S. P., ZHANG, Q-F. & FAETH, G. M. 1984 Structure of particle-laden jets: measurements and predictions. *A.I.A.A.J.* **23,** 396–404.

SUN, T-Y. 1985 A theoretical and experimental study of noncondensible turbulent bubbly jets. Ph.D. Dissertation, The Pennsylvania State University, University Park, PA.

SUN, T-Y. & FAETH, G. M. 1985 Structure of turbulent bubbly jets—II. phase property profiles. *Int. J. Multiphase Flow* **12,** 115–126.

TURNER, J. S. 1969 Buoyant plumes and thermals. *Ann. Rev. Fluid Mech.* **1,** 29–44.

WYGNANSKI, I. & FIEDLER, H. E. 1969 Some measurements in the self-preserving jet. *J. Fluid Mech.* **38,** 577–612.